New insights into biocathode material as a key determinant of electro-methanogenic activity and significance of extracellular polymeric substances

Basem S. Zakaria, Bipro Ranjan Dhar*

Civil and Environmental Engineering, University of Alberta, 9211-116 Street NW, Edmonton, AB, Canada T6G 1H9

Highlights

- Stainless-steel mesh outperformed carbon fibers for methanogenic biocathode.
- Multifaceted characterization of biofilms unveiled underlying mechanisms.
- The results confirmed H_2-utilizing methanogenesis is the dominant pathway.
- Homoacetogenesis only played a crucial role in the stainless-steel biocathode.
- Biocathode EPS might be responsible for superior methanogenesis.

Graphical Abstract

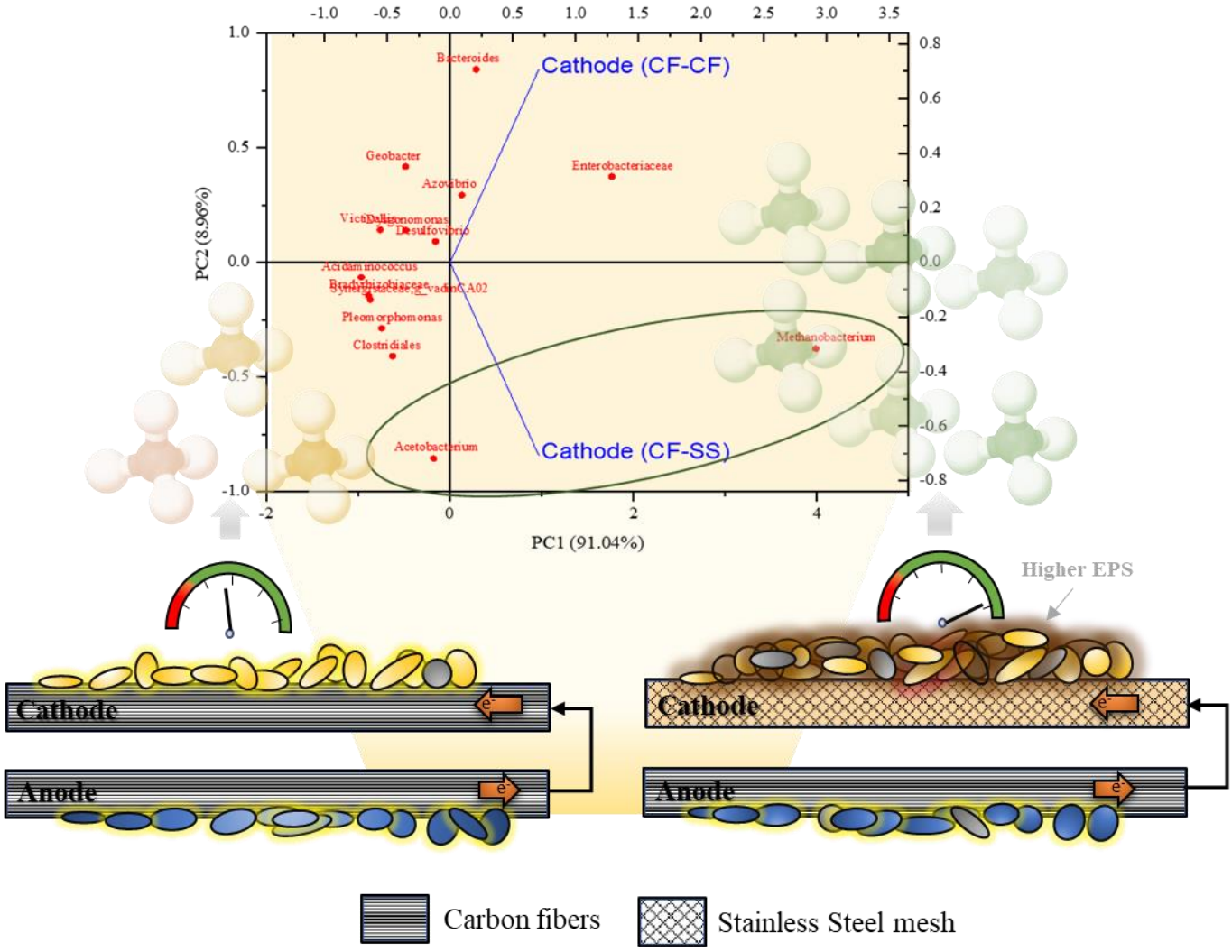

Abstract

Carbon-based electrodes have been mostly used as a biocathode material in microbial electrolysis cell assisted anaerobic digestion (MEC-AD) due to their excellent biocompatibility and higher surface area over metal-based electrodes. Here, we report a multifaceted approach combining characterization of microbial communities, extracellular polymeric substances (EPS), redox oxygen species (ROS), and expression of genes associated with extracellular electron transfer (EET) to shed light on mechanisms governing electro-methanogenic activity in different biocathode materials. Carbon fiber and stainless-steel mesh biocathode were tested in MEC-AD systems fed with synthetic glucose medium. Despite the higher specific surface area provided by carbon fiber biocathode, methanogenesis performance was much inferior (100.3 mL CH_4) than that obtained from a stainless steel biocathode (179.5 mL CH_4). Interestingly, biofilms did not entirely cover the surfaces of carbon fibers, while stainless steel biocathode showed evenly denser biofilms with higher biovolume (30.2±4.2 vs. 13.5±2.8 $\mu m^3/\mu m^2$). Analyses of microbial communities indicated that the key mechanism for electro-methanogenesis in both reactors was hydrogenotrophic methanogenesis by *Methanobacterium* species. The redox activity of EPS derived from biocathode, as well as expressions of EET genes, suggested that electro-methanogenesis via direct electron transfer might have occurred to some extent in both biocathodes. Higher abundance of strictly hydrogenotrophic *Methanobacterium* sp. and homoacetogenic *Acetobacterium* appeared to play a major role in higher methanogenesis performance from stainless steel biocathode. It was possibly attributed to effective catalysis of hydrogen evolution reaction (HER) on stainless steel biocathode. The most considerable secretion of EPS accompanied by the lowest ROS level in stainless steel biocathode indicated that higher EPS possibly protected cells from harsh metabolic conditions (e.g., unfavorable local pH) induced

by faster HER. The results of this study have important significance in the development of effective biocathode for MEC-AD systems.

Keywords: Electro-methanogenesis; Biomethane; Biocathode; Extracellular polymeric substances; MEC-AD

1. Introduction

The concept of electro-methanogenesis by combining the microbial electrolysis cell (MEC) and anaerobic digestion (AD) has become a promising method for process intensification and improving the stability of digesters (Choi et al., 2017; Huang et al., 2020; Park et al., 2018d; Zakaria et al., 2020; Zakaria and Dhar, 2021). The integrated process is called microbial electrolysis cell assisted anaerobic digester (MEC-AD). In MEC-AD systems, methane can be produced via multiple pathways. For instance, methane can be produced in biocathode through (1) direct electron transfer from the electrode to electrotrophic methanogens coupled with CO_2 reduction to methane, and (2) hydrogenotrophic methanogenesis of H_2 produced via hydrogen evolution reaction (HER) (Huang et al., 2020; Villano et al., 2010; Zakaria et al., 2020; Zakaria and Dhar, 2019). Moreover, methane can also be produced via direct interspecies electron transfer (DIET) between electroactive bacteria and electrotrophic methanogens in both cathode and anode electrodes (Siegert et al., 2015, 2014; Zakaria and Dhar, 2019). Nonetheless, a considerable portion of methane would still be generated via conventional acetoclastic and hydrogenotrophic methanogenesis pathways.

The activity of anodic electroactive bacteria (EAB) was identified as one of the key factors for boosting the methanogenesis process in MEC-AD systems. Remarkably, EAB can outcompete acetoclastic methanogens due to faster growth kinetics (Cheng et al., 2009). Thus, EAB can divert electrons from acetate to anode via extracellular electron transport (EET). The transferred electrons

can be utilized for hydrogen production via a cathodic HER. Thus, fast-growing hydrogenotrophic archaea can be augmented on the biocathode. Several studies revealed enrichment of known hydrogenotrophic methanogens, such as *Methanobacterium* and *Methanobrevibacter* in the cathode, which corroborated faster methanogenesis rates in MEC-AD systems over conventional digesters (Cheng et al., 2009; Dykstra and Pavlostathis, 2017; Siegert et al., 2015, 2014).

While many studies emphasized the importance of a kinetically efficient electrode-attached microbiome in MEC-AD systems, studies documented the significance of extracellular polymeric substance (EPS) in biocathode are limited. Biofilm EPS can have many functions, including attachment of cells to solid surfaces, maturation of biofilm structures, and protection of cells from harsh environmental conditions (Xiao et al., 2017; Zakaria and Dhar, 2020; Zhang et al., 2011). A few recent studies validated the significance of EPS in EET within anode biofilms in various bio-electrochemical systems (Rollefson et al., 2011; Tan et al., 2019; Tian et al., 2019; Xiao et al., 2017). In general, EPSs are composed of proteins, DNA, humic acids, polysaccharides, etc., that are secreted by microbes in pure and mixed cultures, which facilitate biofilm growth and protection under unfavorable metabolic environment (Xiao et al., 2017; Zakaria and Dhar, 2020). Notably, various EPS components, including humic acids, extracellular DNA (eDNA), and heme-binding proteins, showed redox properties, which could serve as an immobilized mediator (i.e., electron carrier) in electrochemically active biofilms (Rollefson et al., 2011; Tan et al., 2019; Xiao et al., 2017). Interestingly, EPS extracted from anaerobic digester has now been shown to have redox properties and identified as an essential route for DIET between syntrophic bacteria and electrotrophic methanogens (Ye et al., 2018; Yu, 2020). As direct electron transport from the cathode-to-methanogen and bacteria-to-methanogens can promote methanogenesis in biocathode, it can be assumed that EPS in biocathode can potentially be linked with MEC-AD performance.

However, to the best of the authors' knowledge, there is no published literature reporting the characteristics and significance of biocathode EPS in MEC-AD systems.

The optimization of applied voltage/potential and inoculation method has been broadly investigated to enrich a syntrophically balanced microbial communities towards developing MEC-AD systems (Villano et al., 2016; Zakaria and Dhar, 2021). Previous studies also substantiated the importance of persuasive system design for effective electro-methanogenesis (Guo et al., 2017; Ma et al., 2017; Noori et al., 2020). Particularly, the selection of cathode electrode with low overpotential, large effective surface area, and good conductive properties was found to play a deterministic role in MEC-AD performance (Choi et al., 2017; De Vrieze et al., 2014; Liu et al., 2017, 2016). However, carbon based-cathode materials, such as carbon fiber, carbon cloth, and carbon brush, have been employed in most of the previous studies due to their high surface area and biocompatibility properties (Choi et al., 2017; De Vrieze et al., 2014; Liu et al., 2016). However, carbon-based electrodes provide slow catalysis for cathodic HER, which seems to be critical for enriching hydrogenotrophic methanogens (Kim et al., 2017; Liu et al., 2016; Park et al., 2018d). Some previous studies successfully employed metal catalyst on carbon electrodes, such as nickel- and platinum-coated carbon materials, to provide superior HER (Kim et al., 2017; Liu et al., 2016; Park et al., 2018d), while these catalysts are still quite expensive. In contrast, non-precious metal electrodes, such as stainless steel, have shown an excellent low-cost alternative to promote HER (Call et al., 2009; Dykstra and Pavlostathis, 2017; Liu et al., 2017; Park et al., 2018c; Wang et al., 2016). However, to date, limited information is available on how carbonaceous and metal-based electrodes shape biocathode structures in terms of EPS and microbial communities.

Considering the research gaps mentioned above, the main goal of this study was to provide fundamental insights into the EPS as well as microbial communities that drive methanogenesis in

biocathode developed on carbon and metal electrode surface. To the best of the authors' knowledge, this is one of the first studies to use a multifaceted approach combining molecular biology, microscopic, and electrochemical tools to link the structures and compositions of biocathode EPS and microbial communities with their methanogenesis performance.

2. Materials and methods

2.1. MEC Start-up and operation

Two single chamber MEC-AD systems (working volume of 360 mL), constructed with plexiglass, were used in this experiment. Carbon fibers (2293-A, 24A Carbon Fiber, Fibre Glast Development Corp., Ohio, USA) fixed onto a stainless steel frame (which was not exposed to the liquid medium) was used as an anode electrode in both reactors. A similar carbon fiber module was used as a cathode electrode in one reactor (referred to as 'CF-CF'), and a stainless steel mesh (304 stainless steel, McMASTER-CARR, USA) was used as a cathode electrode in the other reactor (referred to as 'CF-SS'). The specific surface area provided by the stainless-steel electrode was 4.2 m^2/m^3. Considering every single filament in the carbon fiber bundle, the specific surface area of the carbon fibers module was estimated at 3609 m^2/m^3. Moreover, considering all filaments in a bundle act together as a single fiber, the surface area was estimated at 41 m^2/m^3. The detailed calculation of the specific surface areas for carbon fibers and stainless-steel electrodes are provided in the Supplementary Information. The Ag/AgCl reference electrode (MF-2052, Bioanalytical System Inc., USA) was positioned close (<1 cm) to the anode electrode.

Both reactors were inoculated with mesophilic anaerobic digester sludge and effluent from a dual-chamber mother MEC that has been operated with sodium acetate as a sole electron donor for over 12 months. Initially, sodium acetate (1600±55 mg COD/L) supplemented phosphate buffer (50 mM) and trace minerals were used as a substrate. The detailed information regarding the trace

minerals can be found elsewhere (Zakaria and Dhar, 2021). The reactors were operated with acetate in fed-batch mode until peak current densities for both reactors reached ~77 A/m^3. Then, the substrate was switched to glucose (2150±31 mg COD/L), while buffer and trace minerals composition remained the same. With glucose medium, reactors were operated for about six months under batch mode in repetitive cycles. The biogas produced from the reactors were collected into gasbags. A decrease in daily methane production to <3 mL was considered as an indicator for replacing the substrate medium. During experiments, a multi-channel potentiostat (Squidstat Prime, Admiral Instruments, Arizona, USA) was used to fix the anode potential at -0.4 vs. Ag/AgCl. The reactors were operated at room temperature 21±1°C with continuous mixing of the liquid medium with magnetic stirrers at 130±5 rpm.

2.2. Characterization of EPS

For the quantitative analysis of EPS, biomass samples were washed three times with 0.1 M PBS (pH 7.4), and then the supernatant was removed after centrifugation at 3000 × g for 15 min at 21°C. EPS extraction was performed using two methods; cation-exchange resin (CER) and heating method, to examine the effect of different EPS extraction methods. The details of EPS extraction and analytical methods for various EPS components (proteins, carbohydrates, eDNA, heme-binding proteins, and uronic acid) were provided in the Supplementary Information. Both EPS extraction methods (CER and heating method) provided similar results (see Supplementary Information). Hence, we reported the results from the CER method.

Confocal laser scanning microscopy (CLSM) was used to visualize and examine the EPS structure on the electrodes. Portions of carbon fibers and stainless-steel mesh were cut with an aseptic scissor from different locations and washed with 0.1 M PBS buffer (pH 7.4) to remove any debris. The electrodes were fluorescently stained with TOTO^{TM}-1 (Thermo Fisher, USA) and Concanavalin A

(ConA) Alexa Fluor™ 633 Conjugate (Thermo Fisher, USA) for one hour in the dark for eDNA and EPS visualization, respectively. Then, the samples were washed again with PBS buffer to remove any non-specific binding stains. The stained electrodes were placed on MatTek dishes with a 1.5 coverslip (MatTek co., USA) to ensure that the biofilm was not compressed. The visualization of the electrodes was performed using a Leica inverted DMI 6000 B microscope (Leica Microsystems, USA). CLSM was equipped with an argon laser and helium-neon lasers. The images were acquired using x63/1.3 water immersion lens using LAS AF software (Leica Microsystems, USA) at a resolution of 1024 x 1024 with 120 nm pixel size. Images z-stack were acquired with several steps 29 with z-step size 0.29 µm with smart grain 687. The quantitative analysis of EPS structure was carried out using biofilm image processing COMSTAT software. The EPS intensities were reported as intensity/um^3 of the electrode.

The electrochemical characteristics of extracted EPS from cathodic biofilms was further analyzed with low-scan cyclic voltammetry under three-electrode (working, counter, and reference) configuration. After extraction, 2 mL of extracted EPS was transferred to an electrochemical cell having screen printed electrodes (A-AD-GG-103-N, Zimmer and Peacock Ltd., Royston, UK). The working electrode voltage was ramped between −0.8 and 0.8 V vs. Ag/AgCl at a scan rate of 1 mV/s using the potentiostat (Squidstat Prime, Admiral Instruments, USA), and current was recorded every 1 seconds.

2.3. Microscopic imaging of biofilms

Microscopic visualization of anode and cathode biofilms was performed using a scanning electron microscope (Carl Zeiss, Cambridge, UK). Several images from different locations of electrodes were captured. The detailed protocol of sample preparation and imaging could be found elsewhere (Zakaria and Dhar, 2020).

2.4. Analysis of reactive oxygen species (ROS)

The levels of reactive oxygen species (ROS) in biofilms were visualized using CLSM. We collected different parts of electrodes, then washed three times using 0.1 M PBS to remove any debris. Samples were stained with 2',7'-Dichlorofluorescein diacetate (10 µM) (Thermo Fisher, USA) for one hour. The visualization was then performed using CLSM (as mentioned earlier) with excitation and emission wavelength; 495 nm and 520 nm, respectively. The quantitative analysis of ROS levels was carried out using image processing COMSTAT software.

2.5. Microbial communities and gene expression analyses

For the characterization of microbial communities, genomic DNA was extracted using PowerSoil® DNA Isolation Kit (MoBio Laboratories, Carlsbad, USA) according to the manufacturer's instructions from the anode and cathode biofilm. The purity and concentration of DNA was measured with Nanodrop spectrophotometer (Model 2000C, Thermo Scientific, USA). The extracted DNA was stored immediately at -70 ˚C prior to the sequencing. Illumina Miseq Sequencing was performed by the Research and Testing Laboratory (Lubbock, TX, USA) targeting 16S rRNA gene using bacterial primers 341F: 5' CCTACGGGNGGCWGCAG 3' and 805R: 5' GACTACHVGGGTATCTAATCC 3' (Klindworth et al., 2013; Logares et al., 2013), archaeal primers 517F: 5' GCYTAAAGSRNCCGTAGC 3' and 909R: 5' TTTCAGYCTTGCGRCCGTAC 3' and specific *mcr*A archaeal primers *mcr*Af: 5' GGTGGTGTMGGATTCACACARTAYGCWACAGC 3' and *mcr*Ar: 5' TTCATTGCRTAGTTWGGRTAGTT 3' (Morris et al., 2014).

For evaluation of microbial diversity, the nucleotide sequence reads were sorted out using a data analysis pipeline. Short sequences, noisy reads and chimeric sequences were removed through a denoising step and chimera detection, respectively. Then, each sample was run through the

analysis pipeline to establish the taxonomic information for each constituent read. Microbial taxonomy was assigned using the Quantitative Insights Into Microbial Ecology (QIIME) pipeline (http://qiime.org; Caporaso et al., 2010). Principal component analysis (PCA) of bacterial and archaeal communities on cathode electrodes of CF-CF and CF-SS was conducted using weighted Unifrac metrics to show the relation between genera and PCs.

The expression of EET-associated genes (i.e., *pil*A, *omc*B, *omc*C, *omc*E, *omc*Z, and *omc*S) were quantified. The primers and design method used in this study are listed in the Supplementary Information. Total RNA was extracted using RNeasy PowerSoil Total RNA Kit (Qiagen, CA), then the purity and concentration were examined using Nanodrop (2000C, Thermo Scientific, USA). Subsequently, cDNA synthesis was performed using QuantiTect Reverse Transcription Kit (Qiagen, CA). Then, RT-PCR mixtures were prepared in 25 uL reactions using QuantiFast SYBR® Green PCR Kit (Qiagen, CA) as the following: 1 µL of the template, 12.5 µL 2x master mix, 2.5 µL forward and reverse specific primer, and 6.5 µL nuclease-free water. CFX 96 real-time PCR system with a C1000 Thermal Cycler (Bio-Rad, USA) was used with the following cycling conditions according to the QuantiFast SYBR® Green PCR Kit's protocol; PCR initial heat activation cycle at 95 ˚C for 5 min, 35 cycles at 95 ˚C for 10 sec and 60 ˚C for 30 sec, and finally, one cycle at 40 ˚C for 30 seconds. Triplicate reactions were run for all samples.

2.6. Analytical methods

Current and applied voltage/potential were recorded every 4.8 min using a computer connected with the multi-channel potentiostat (Squidstat Prime, Admiral Instruments, USA). The liquid samples from reactors were filtered with syringe filters (0.45 µm) for chemical oxygen demand (COD) measurements. The COD concentrations were measured with HACH Chemical method using UV-spectrophotometer (Model DR 3900, HACH, Germany). A bench-top pH meter

(Accumet AR15, Fisher Scientific, Pittsburgh, PA, USA) used for pH measurment. The concentrations of various volatile fatty acids, VFAs (acetate, propionate, and butyrate) were measured with an ion chromatography (DionexTM ICS-2100, Thermo Scientific, USA); the detailed operating protocol could be found elsewhere (Zakaria et al., 2019). The biogas produced from reactors was collected with 500 mL gas bags. The composition of biogas (i.e., methane content) was analyzed by a gas chromatograph (7890B, Agilent Technologies, Santa Clara, USA) equipped with a thermal conductivity detector (TCD) and two columns (Molsieve 5A and Hayesep).

2.7. Statistical analysis

To reveal the statistical difference between the data collected from CF-CF and CF-SS reactors, the student's paired t-test (JMP® Software, SAS, US) was used.

3. Results and discussion

3.1. MEC-AD performance

The performances of MEC-AD systems were compared in terms of current density and methane productivity. Fig. 1a shows the volumetric current densities from two configurations. The maximum volumetric current density from the CF-SS reactor reached 34.1±0.3 A/m^3, which was significantly higher (p=0.01) than that of CF-CF (27.6±0.2 A/m^3). Fig. 1b shows the methane production profiles during batch operation. Although the methane production patterns were comparable in both reactors, CF-SS showed higher (p=0.03) daily methane production than CF-CF throughout the batch cycle (Fig. 1b). Also, the total cumulative methane production was substantially higher in CF-SS (179.5±6.7 vs. 100.3±7.9 mL CH_4; p=0.01). Both reactors were operated under identical operating conditions. Furthermore, considering that the carbon fibers

module was used as the anode electrode in both reactors, the differences in system performance could be closely tied to the difference in the cathode electrode. As discussed later, stainless steel mesh cathode in the CF-SS reactor facilitated denser biofilms formation with more methanogenic biomass with higher EPS levels.

It is interesting to note that electrodes providing high specific surface areas have been reported to be efficient for enhancing the electrochemical performance of various bio-electrochemical systems (Choi et al., 2017; De Vrieze et al., 2014; Guo et al., 2017; Liu et al., 2017, 2016). Therefore, carbon-based electrodes, such as carbon brush, activated carbon, have been widely used for various biocathode applications, including electro-methanogenesis (Choi et al., 2017; De Vrieze et al., 2014; Liu et al., 2016). Notably, the rough surface of carbon fiber was found to be efficient for developing electrochemically active biofilms (Li et al., 2017). Although we cannot rule out that different textures (diameter of carbon fiber and steel wire) could also lead to distinct colonization of biomass (Champigneux et al., 2018; He et al., 2011), the specific surface area provided by electrodes is often considered a critical factor in designs of bio-electrochemical systems. It appeared that stainless steel mesh cathode having a relatively lower specific surface area than carbon fibers (4.23 vs. 3609 m^2/m^3) resulted in superior methanogenic activity from CF-SS. It has been previously suggested that the agglomeration of fibers in the liquid phase could reduce the available specific surface area for biofilms formation (Babapoor et al., 2015). Nonetheless, considering all carbon fiber filaments in a bundle as a single fiber, the specific surface area provided by the carbon fiber biocathode was still higher than the stainless-steel cathode (4.23 vs. 41 m^2/m^3).

Carbon-based electrodes are considered inferior catalysts for HER compared to metal and carbon-metal composite electrodes (Call et al., 2009; Dykstra and Pavlostathis, 2017; Liu et al., 2017;

Park et al., 2018c; Wang et al., 2016). Most of the previous single-chamber MEC-AD studies substantiated the role of hydrogenotrophic methanogenesis on the biocathode. Also, it is reasonable that acetoclastic methanogens would likely be washed out at low hydraulic residence time (<7 days) used in this study (Gaby et al., 2017; Zakaria and Dhar, 2019). Thus, the inferior methane recovery from the CF-CF reactor as compared to the CF-SS reactor was likely due to the inferior catalytic activity of carbon fibers for HER and subsequent indirect electro-methanogenesis (i.e., hydrogenotrophic methanogenesis of hydrogen produced via HER).

3.2. Organics removal and VFAs profiles

As shown in Fig. 2a, the effluent COD concentration from CF-SS (215±2.8 mg/L) was considerably lower (p=0.001) than that of CF-CF (382±3.0 mg/L). Correspondingly, the COD removal efficiencies were 89.9±0.5% and 83±1.7% in CF-SS and CF-CF, respectively. Thus, the COD removal efficiencies also showed similar trends with volumetric current density and methane production. Fig. 2b and 2c show the changes in VFAs concentrations during batch operation. For both reactors, the acetate concentrations were relatively higher than propionate and butyrate concentrations during the operational period. The CF-SS reactor showed the highest acetate concentration of 439±2 mg COD/L, while propionate (94±0.1 mg COD/L) and butyrate (61±0.3 mg COD/L) concentrations were relatively lower. In contrast, CF-CF exhibited the highest acetate concentration of 320±0.4 mg COD/L, which was lower than that of the highest acetate concentration observed in CF-SS. Propionate concentrations were relatively higher in CF-CF, with the highest concentration of 118±0.4 mg COD/L. The highest butyrate concentration (64.8±1.3 mg COD/L) in CF-CF was comparable to CF-SS (61±0.3 mg COD/L). CF-SS also showed a lower accumulation of VFAs in the final effluent, as compared to CF-CF (52.6±0.5 vs. 133.5±1.0 mg COD/L; p=0.005).

Throughout the batch operation, propionate concentrations in CF-SS remained relatively lower than those observed in CF-SS, indicating faster conversion of propionate in the CF-SS. The fermentation of propionate to acetate is a vital process towards anodic respiration by EAB as well as acetoclastic methanogenesis. However, propionate fermentation to acetate is energetically unfavorable in terms of Gibbs free energy (Krylova and Conrad, 1998). Thus, maintaining lower hydrogen partial pressure would be critical for propionate fermentation to acetate. Even though stainless-steel cathode would be expected to provide superior HER compared to the carbon fibers (Call et al., 2009; Dykstra and Pavlostathis, 2017), no hydrogen was detected in biogas collected from both reactors. This might be due to the rapid consumption of hydrogen by hydrogenotrophic methanogens, as suggested in previous studies (Asztalos and Kim, 2015; Dykstra and Pavlostathis, 2017). Moreover, enhanced homoacetogenic activity ($H_2 + CO_2 \rightarrow$ acetate) could play a role in maintaining lower hydrogen partial pressure in biocathode (Asztalos and Kim, 2015; Dykstra and Pavlostathis, 2017). As discussed later, microbial community analysis also coincided with these notions. Thus, the comparison of VFA profiles suggests that microbial communities in the CF-SS reactor more rapidly utilized hydrogen produced via fermentation and cathodic HER.

3.3. EPS structures and characteristics

Fig. 3 shows that carbohydrates, proteins, and heme-binding proteins were the major components of EPS extracted from biofilms in both reactors. The EPS composition of the anode biofilms in both reactors was quite similar and was not affected by the differences in the cathode electrode between the two configurations. Protein was found as the major EPS component in anode biofilms in this study, which is consistent with recent reports on EPS composition in pure culture *Geobacter* biofilms (Stöckl et al., 2019; Tan et al., 2019). *Geobacter* species were also abundant in anode biofilms of both reactors in this study (discussed later). The concentrations of major EPS

components (carbohydrates, proteins, and hemes) in the cathode biofilms in CF-SS were higher than those of CF-CF. Notably, carbohydrates (52.2±0.2 mg/cm^2) and proteins (212.8±3.4 mg/cm^2) concentrations were markedly higher in CF-SS, as compared to cathode biofilms in CF-CF (carbohydrates: 25.8±0.5 mg/cm^2; proteins: 170±1.3 mg/cm^2). The heme-binding proteins (CF-CF: 16.5±0.4 mg/L; CF-SS: 34.2±2.3 mg/L), uronic acid (CF-CF: 6.2±1.0 mg/L; CF-SS: 15±0.2 mg/L) and eDNA (CF-CF: 0.39±0.01 mg/L; CF-SS: 1.5±0.05 mg/L) also showed same patterns. Overall, cathodic biofilms developed on the stainless-steel electrode exhibited markedly higher EPS levels ($p=0.03$).

To further verify EPS measurement results, electrode surfaces were visualized with CLSM (see Fig. 4) to quantify EPS intensity and biovolume of biofilms. The CLSM images showed that EPS was more uniformly distributed on the stainless-steel cathode surface in CF-SS than the carbon fiber electrodes in both reactors. As shown in Fig. 5a, the biovolume of cathode biofilms in CF-SS was estimated at 30.2±4.2 μm^3/μm^2, which was two times higher than the biovolume estimated for cathode biofilms in CF-CF (13.5±2.8 μm^3/μm^2). However, biovolumes estimated for anode biofilms in both reactors were comparable ($p=0.007$). The intensities of EPS and eDNA were also quantified (Fig. 5b). Like estimated biovolume, EPS and eDNA intensities in cathode biofilms on stainless steel were higher than those estimated for cathode biofilms in the CF-CF reactor ($p=0.008$). At the same time, EPS and eDNA intensities were comparable for anode biofilms in both reactors ($p=0.20$). Thus, CLSM imaging and COMSTAT analysis further confirmed that the stainless-steel cathode resulted in the highest EPS production.

Studies associated with the role of EPS in the performance of bio-electrochemical systems received less attention and primarily focused on anode biofilms and their interrelationships with electrocatalytic activity (i.e., current density). A few studies revealed that EPS extracted from

biofilms of electroactive *Geobacter sulfurreducens*, *Shewanella oneidensis* and *Pseudomonas putida* were electrochemically active (Stöckl et al., 2019; Tan et al., 2019; Xiao et al., 2017). Notably, EPS-associated proteins with redox-active features are a significant contributor to the EET from EAB to the anode (Stöckl et al., 2019; Tan et al., 2019; Xiao et al., 2017). Moreover, higher levels of redox-active proteins in anode biofilms were correlated with higher EET efficiency. Interestingly, despite differences in volumetric current densities, both EPS composition and concentrations were quite similar in anode biofilms in both reactors. Instead, the difference in EPS levels in cathode biofilms was likely linked to volumetric current densities and methane production. Interestingly, a recent study demonstrated that the addition of iron-based conductive materials in conventional anaerobic bioreactors could enhance EPS contents in methanogenic biomass (Ye et al., 2018), which was positively correlated with methane generation rates. Conductive materials promote the syntrophic DIET from bacteria to archaea and thereby enhance methanogenesis (Park et al., 2018a). Therefore, to get more insights, the CV of extracted EPS was performed to qualitatively identify the redox activity of cathodic EPS. As shown in Fig. 6, voltammograms of cathodic EPS extracted from both reactors showed distinct redox peaks, suggesting the redox capability of EPS in both biocathodes. However, redox peaks were observed at different potential, indicating that redox properties would be different for EPS extracted from different cathode electrodes. Moreover, the peak current from the EPS extracted from stainless steel biocathode was considerably higher than the EPS extracted from carbon fiber biocathode. This difference could be associated with higher concentrations of redox-active EPS in stainless steel biocathode; however, future investigation is warranted to reach a more thorough understanding of their redox characteristics.

A recent study reported that the current generated from anode biofilms was positively associated with EPS protein content and negatively correlated to carbohydrates in EPS (Yang et al., 2019). In this study, both carbohydrates and proteins were considerably higher in EPS extracted from stainless steel biocathode than that of carbon fiber biocathode. The secretion of carbohydrates could be associated with harsh environmental conditions (Yu, 2020; Zakaria and Dhar, 2020). More secretion of carbohydrates can provide a protective layer and maintain the redox activity of proteins involved in EET (Rollefson et al., 2011; Yu, 2020). It is possible that enhanced HER with a stainless steel cathode could create highly alkaline conditions near the cathode surface (Cai et al., 2018; Cerrillo et al., 2016; Zakaria and Dhar, 2019), which might induce more EPS secretion. Based on a recent report, hydrogenotrophic methanogenesis could be the dominant pathway under alkaline pH (Wormald and Humphreys, 2019). As discussed later, biofilms grown on stainless steel cathode showed a higher abundance of hydrogenotrophic methanogens in this study. While further investigation is needed to understand the function of various EPS on electro-methanogenesis, the results suggested that cathodic electrode material could considerably influence biofilm growth/composition along with EPS secretion, and ultimately the methane productivity and kinetics from MEC-AD systems.

3.4. ROS levels in biofilms

The quantitative measurement of ROS levels in biofilms was performed with CLSM imaging (see Supplementary Information), which showed a difference in the ROS level between biofilms grown on stainless steel and carbon fibers (Fig. 7). The lowest ROS level was observed for cathode biofilms on stainless steel surface, while very similar ROS levels were found in anode/cathode biofilms developed on carbon fibers. Recent studies reported ROS accumulation in the anaerobic digestion process (Tian et al., 2019; Zheng et al., 2019), while ROS is usually thought to be

produced during aerobic metabolism. It has been suggested that unfavorable metabolic conditions (e.g., inhibition by toxicants, pH changes) could lead to ROS accumulation in digesters (Tian et al., 2019; Zheng et al., 2019). For instance, superior HER on stainless steel could induce local alkaline pH in biocathode. ROS accumulation may suppress metabolic activities, leading to the deterioration of digester performance. The lowest ROS level in biocathode developed on stainless steel suggests that higher EPS levels provided some degree of protection to the cathodic microbiome from potential environmental stress (e.g., pH changes). However, potential mechanisms relating to EPS and ROS levels should be further explored.

3.5. Microbial quantity and diversity

Fig. 8 shows the quantitative assessment of microbial communities performed with qPCR. The total microbial cell counts (16S) in anode biofilms in CF-SS (9×10^8 cells/cm^2) were slightly higher than that of CF-CF (8×10^8 cells/cm^2) (Fig. 8a). An almost similar pattern was observed for cathode biofilms; however, the difference was more prominent (CF-SS: 1×10^{11} cells/cm^2; CF-CF: 6×10^8 cells/cm^2). The archaeal cell numbers also showed similar patterns, with the highest archaeal cell numbers for the stainless steel biocathode. In addition, *mcr*A gene copies were quantified to elucidate the archaeal cell numbers; the *mcr*A gene is considered as a biomarker for methanogens (Wilkins et al., 2015). Sequencing of the *mcr*A gene was used in a few studies to understand the taxonomy of methanogens (Alonso et al., 2020; Morris et al., 2014; Wilkins et al., 2015). A few recent reports also confirmed the positive link between *mcr*A gene copies and methanogenesis rates in MEC-AD reactors (Alonso et al., 2020; Morris et al., 2014; Wilkins et al., 2015). The highest *mcr*A gene copy numbers were observed for the cathodic biofilm in CF-SS (4×10^6 cells/cm^2), as compared to the CF-CF reactor (4×10^4 cells/cm^2) (Fig. 8b). The *mcr*A gene copy numbers in anodic biofilms for both systems were comparable (CF-CF: 1.3×10^4 cells/cm^2; CF-SS:

1.8×10^4 cells/cm^2). Thus, the enhanced methane recovery from the CF-SS reactor can be explained by the higher abundance of *mcr*A gene copies within the stainless steel biocathode.

Fig. 10 shows microscopic images of biofilms, which show the differences in structures of biofilms developed on different electrodes. The anode/cathode biofilms grown on carbon fibers exhibited substantial heterogeneity (Fig. 10). Also, it can be clearly noticed that biofilms did not fully cover the surfaces of carbon fibers. SEM imaging revealed that biofilms grown on stainless steel cathode in CF-SS was evenly denser than anode/cathode biofilms grown on carbon fiber electrodes (Fig. 10), suggesting the large secretion of EPS accelerated the surface attachment of cells on the stainless steel electrode. Thus, SEM imaging also corroborates the qPCR and CLMS results.

The alpha diversity of anode and cathode biofilms was also estimated. The numbers of Chao 1, phylogenetic distance, OTUs, Pielou's evenness, and Shannon index were provided in the Supplementary Information. The results clearly showed that the richness and diversity indices were relatively higher in CF-SS. Notably, cathode biofilms in CF-SS showed more diversity with the Shannon index of 5.10, as compared to CF-CF (3.95). These results indicated that the stainless-steel electrode persuaded the richness and diversity of the microbial communities.

3.6. Microbial community composition, and gene expression

3.6.1. 16S rRNA sequencing

Microbial communities in two reactors were analyzed with specific bacterial, archaeal, and *mcr*A primers. At the phylum level, Proteobacteria was the most abundant in anode biofilms in both reactors; however, its relative abundance was much higher in CF-SS than CF-CF (85% vs. 47%) (see Supporting Information). The relative abundances of Bacteroidetes and Firmicutes in CF-CF were 26% and 14%, which were considerably higher than that of CF-SS (6% and 4%, respectively).

Also, Synergistetes (6%) and Lentisophaerae (4%) were present at slightly higher abundances in CF-CF, while in CF-SS, they were 1% and 3%, respectively. Similar to anode biofilms, Proteobacteria was the most abundant in cathode biofilms in both reactors. However, its relative abundance was comparable in both configurations; recorded 64% and 68% of CF-CF and CF-SS, respectively. However, the abundance of Bacteroidetes was higher in CF-CF (17%) than CF-SS (6%). On the contrary, Firmicutes (20%) was the second most abundant member in CF-SS, while their abundance in CF-SS was considerably lower (9%).

At the genus level, *Geobacter*, belong to Proteobacteria, was the most abundant in anode biofilms in both systems with 22% and 59% in CF-CF and CF-SS, respectively (Fig. 9a). *Geobacter* is a highly efficient electroactive microorganism that has the capability to utilize simple organic acids like acetate and were widely dominant on the anode biofilm in most of the previous studies (Dhar et al., 2016; Malvankar et al., 2012). In CF-CF, *Bacteroides* was the second most dominant genus (12%), followed by *Enterobacteriaceae* (10%) and *Dysgonomonas* (5%). In contrast, the second abundant genus in CF-SS was *Enterobacteriaceae* (23%), followed by *Dysgonomonas* (3%) and *Victivallis* (3%).

The cathode biofilms in both reactors are dominated by the members of *Enterobacteriaceae* genus (CF-CF: 42%; CF-SS: 60%). On the cathode electrodes, *Bacteroides* (12%), *Pleomorphomonas* (9%), and *Desulfovibrio* (4%) were the other dominant genera in CF-CF. In contrast, *Acetobacterium* was the second abundant genus (16%), followed by *Bacteroides* (5%), *Dysgonomonas* (3%), and *Desulfovibrio* (2%) in CF-SS. *Acetobacterium*, known homoacetogenic bacteria, can utilize H_2 and CO_2 to produce acetate (Dhar et al., 2019; Liu et al., 2017). Then, acetate can be consumed by either acetoclastic archaea or anodic electroactive bacteria (Cheng et al., 2009; Fu et al., 2015; Zakaria and Dhar, 2019). The enrichment of *Acetobacterium* on the

stainless-steel mesh cathode electrode is an indicator to the occurrence of high HER in CF-SS, as compared to CF-CF. As mentioned earlier, H_2 gas has not been observed in the biogas samples in this study. This might be due to the rapid utilization of the generated H_2 via hydrogenotrophic methanogens or homoacetogenic *Acetobacterium*, as suggested in the literature (Asztalos and Kim, 2015; Dykstra and Pavlostathis, 2017). In addition, the presence of the highest acetate concentration (439±2 mg COD/L) in CF-SS collaborated with a higher abundance of *Acetobacterium*. Moreover, *Acetobacterium* can help to maintain a lower hydrogen partial pressure to provide thermodynamically favorable conditions for propionate and butyrate fermentation to acetate. This notion is also supported in part by the lower propionate concentrations in CF-SS compared to the CF-CF.

3.6.2. Archaeal primer sequencing

For the archaeal phylum sequenced using specific archaeal primers, the abundance of Euryarchaeota were 32% and 51% at CF-CF and CF-SS, respectively (see Supporting Information). At the genus level, the abundance of *Methanobacterium* was almost similar in the anode biofilms of CF-CF and CF-SS (13% vs. 14%) (see Fig. 9b). However, *Methanobacterium* in cathode biofilms of CF-SS represented higher abundance than CF-CF (51% vs. 32%). Several studies revealed enrichment of known hydrogenotrophic methanogens, such as *Methanobacterium* and *Methanobrevibacter* in the cathode, which corroborated faster methanogenesis rates in MEC-AD systems over conventional digesters (Cheng et al., 2009; Dykstra and Pavlostathis, 2017; Siegert et al., 2015, 2014). The superior HER kinetics on the stainless-steel cathode electrode (CF-SS) could enrich more hydrogenotrophic methanogens in CF-SS. Thus, the enhanced methane recovery from the CF-SS reactor can be explained by the high enrichment of *Methanobacterium*.

3.6.3. *mcr*A primer sequencing

Moreover, *mcr*A gene sequencing was performed to investigate the diversity and phylogeny of methanogens in both systems (Fig. 9c). The sequencing of the *mcr*A gene has been used previously in a few studies to understand the taxonomy of methanogens (Alonso et al., 2020; Morris et al., 2014; Wilkins et al., 2015). For the anodic biofilms, the abundance of *Methanobacterium* species were almost similar, including *formicicum* (CF-CF 67% vs. CF-SS 71%), and *subterraneum* (CF-CF 34% vs. CF-SS 29%). For the cathodic biofilms, CF-SS showed more diverse species of *Methanobacterium*; *formicicum* (54%), *subterraneum* (24.4%), and *palustre* (22%), as compared to CF-CF; *formicicum* (81%), and *subterraneum* (19%). Based on previous reports, electrotrophic activity of various species from the genus *Methanobacterium* is still uncertain (Batlle-Vilanova et al., 2015; Rotaru et al., 2014; Xu et al., 2014). Thus, the presence of diverse species of strict hydrogenotrophic *Methanobacterium* on CF-SS may have contributed to the faster utilization of hydrogen.

3.6.4. Principal component analysis

Fig. 11 shows the PCA analysis of biocathode bacterial and archaeal communities in two reactors using weighted Unifrac metrics to show the relation between genera and PCs. Based on 16S rRNA primer for bacterial sequencing of biocathode, the better performance of CF-SS was directly related to the enrichment of homoacetogenic *Acetobacterium* (Fig. 11a). However, the other genera might have an indirect relation to the superior performance of CF-SS. Based on specific archaeal primer for archaeal sequencing of biocathode, hydrogen-consuming *Methanobacterium* and *Acetobacterium* primarily contributed to the superior performance of CF-SS (Fig. 11b).

3.6.5. Expression patterns of EET genes

Fig. 12 shows the gene expression for *pil*A and c-type cytochromes (*omc*B, *omc*C, *omc*E, *omc*Z, and *omc*S). These genes showed trivial differences in expression levels in anode biofilms between

both reactors, suggesting that higher current density from the CF-SS reactor was not attributed to the overexpression of genes regulating anodic EET. The EET from EAB to the anode has been demonstrated to be facilitated via c-type cytochromes and conductive nanowire or pili (Hernández-Eligio et al., 2020), while fundamental aspects of EET mechanisms in methanogenic biocathode (i.e., direct electron transport from the electrode to methanogens) is still not well understood. Previous reports postulated that conductive pili and c-type cytochromes could play an important role in EET to electrotrophic methanogens from DIET-partners (i.e., electroactive bacteria) (Park et al., 2018b; Rotaru et al., 2014). Based on the authors' knowledge, this study also first reports the expression of EET genes for methanogenic biocathode. Compared to anode biofilms, the EET-associated genes were less expressed in cathode biofilms in both reactors. Previous studies reported that some bacteria (e.g., *Enterobacteriaceae*, *Desulfovibrio*, etc.) found in cathode biofilms in this study could express different cytochromes and/or conductive pili (Gardy et al., 2003; Hernández-Eligio et al., 2020). The expression of these genes was quite comparable in both carbon fibers and stainless-steel cathode electrodes. Thus, the regulations of the EET genes were not affected by different electrode materials and were closely similar in expression levels. Hence, we can consider that differences in performances (i.e., current density, methane production) between two systems may be correlated to the HER and hydrogen utilization kinetics.

4. Conclusions

Here, we probed the multifaceted characteristics of methanogenic biocathode developed on carbon and metal electrode to reveal potential mechanisms regulating their performance. While carbon fibers provided a higher specific surface area, stainless steel mesh outperformed carbon fibers as a biocathode. The results differ from our existing approach to designing MEC-AD systems by providing a high specific surface area of electrodes. Putting together results from microbial

communities, EPS, ROS, and gene expression patterns, effective catalysis of HER on stainless steel cathode was appeared to be the primary reason behind the superior methanogenesis performance. However, gene expression patterns and redox activity of biocathode-derived EPS provided evidence that cathodic EET was also involved in methanogenesis in both biocathodes. Interestingly, homoacetogenesis appeared to be triggered by elevated HER on stainless steel cathode and served as a critical factor balancing HER, fermentation of metabolites (i.e., propionate), and methanogenesis process. It is known that proton reduction to hydrogen during HER will prompt local alkaline pH on the cathode. Hence, we can speculate that higher EPS secretion in stainless steel biocathode could be linked with protecting cells from pH changes, as evidenced by the lowest ROS level. In all, the stainless-steel electrode improved electro-methanogenic efficiency by promoting a higher abundance of H_2-utilizing archaea and homoacetogens. Given that most of the single-chamber MEC-AD studies used carbon-based biocathode, the results of this study are significant for selecting efficient biocathode material to realize improved performance. The results also provide new insights and suggest the importance of biocathode EPS as a potential hotspot for further investigation.

Acknowledgements

This work was supported by the Discovery Grant from Natural Sciences and Engineering Research Council of Canada (NSERC) and the Early Career Research Award from Future Energy Systems (FES). Basem Zakaria acknowledges Killam Trusts for Izaak Walton Killam Memorial Scholarship for his doctoral studies at the University of Alberta.

Contribution Statement

Basem S. Zakaria: Conceptualization, experiment, data analysis, writing - original draft, review/edit; **Bipro Ranjan Dhar:** Conceptualization, funding acquisition, project administration, supervision, writing/review/edit

Notes

The authors declare no competing financial interest.

References

Alonso, R.M., Escapa, A., Sotres, A., Morán, A., 2020. Integrating microbial electrochemical technologies with anaerobic digestion to accelerate propionate degradation. Fuel 267, 117158.

Asztalos, J.R., Kim, Y., 2015. Enhanced digestion of waste activated sludge using microbial electrolysis cells at ambient temperature. Water Res. 87, 503–512.

Babapoor, A., Azizi, M., Karimi, G., 2015. Thermal management of a Li-ion battery using carbon fiber-PCM composites. Appl. Therm. Eng. 82, 281–290.

Batlle-Vilanova, P., Puig, S., Gonzalez-Olmos, R., Vilajeliu-Pons, A., Balaguer, M.D., Colprim, J., 2015. Deciphering the electron transfer mechanisms for biogas upgrading to biomethane within a mixed culture biocathode. RSC Adv. 5, 52243–52251.

Cai, W., Liu, W., Zhang, Z., Feng, K., Ren, G., Pu, C., Sun, H., Li, J., Deng, Y., Wang, A., 2018. mcrA sequencing reveals the role of basophilic methanogens in a cathodic methanogenic community. Water Res. 136, 192–199.

Call, D.F., Merrill, M.D., Logan, B.E., 2009. High surface area stainless steel brushes as cathodes in microbial electrolysis cells. Environ. Sci. Technol. 43, 2179–2183.

Caporaso, J.G., Kuczynski, J., Stombaugh, J., Bittinger, K., Bushman, F.D., Costello, E.K., Fierer, N., Peña, A.G., Goodrich, J.K., Gordon, J.I., Huttley, G.A., Kelley, S.T., Knights, D., Koenig, J.E., Ley, R.E., Lozupone, C.A., McDonald, D., Muegge, B.D., Pirrung, M., Reeder, J., Sevinsky, J.R., Turnbaugh, P.J., Walters, W.A., Widmann, J., Yatsunenko, T., Zaneveld, J., Knight, R., 2010. QIIME allows analysis of high-throughput community sequencing data. Nat. Methods 7, 335–6.

Cerrillo, M., Viñas, M., Bonmatí, A., 2016. Overcoming organic and nitrogen overload in thermophilic anaerobic digestion of pig slurry by coupling a microbial electrolysis cell. Bioresour. Technol. 216, 362–372.

Champigneux, P., Delia, M.L., Bergel, A., 2018. Impact of electrode micro- and nano-scale topography on the formation and performance of microbial electrodes. Biosens. Bioelectron.

Cheng, S., Xing, D., Call, D.F., Logan, B.E., 2009. Direct biological conversion of electrical current into methane by electromethanogenesis. Environ. Sci. Technol. 43, 3953–3958.

Choi, K.S., Kondaveeti, S., Min, B., 2017. Bioelectrochemical methane (CH4) production in anaerobic digestion at different supplemental voltages. Bioresour. Technol. 245, 826–832.

De Vrieze, J., Gildemyn, S., Arends, J.B.A., Vanwonterghem, I., Verbeken, K., Boon, N., Verstraete, W., Tyson, G.W., Hennebel, T., Rabaey, K., 2014. Biomass retention on electrodes rather than electrical current enhances stability in anaerobic digestion. Water Res. 54, 211–221.

Dhar, B.R., Park, J.H., Park, H.D., Lee, H.S., 2019. Hydrogen-based syntrophy in an electrically conductive biofilm anode. Chem. Eng. J. 359, 208–216.

Dykstra, C.M., Pavlostathis, S.G., 2017. Methanogenic Biocathode Microbial Community Development and the Role of Bacteria. Environ. Sci. Technol. 51, 5306–5316.

Fu, Q., Kuramochi, Y., Fukushima, N., Maeda, H., Sato, K., Kobayashi, H., 2015. Bioelectrochemical Analyses of the Development of a Thermophilic Biocathode Catalyzing Electromethanogenesis. Environ. Sci. Technol. 49, 1225–1232.

Gaby, J.C., Zamanzadeh, M., Horn, S.J., 2017. The effect of temperature and retention time on methane production and microbial community composition in staged anaerobic digesters fed with food waste. Biotechnol. Biofuels 10, 302.

Gardy, J.L., Spencer, C., Wang, K., Ester, M., Tusnády, G.E., Simon, I., Hua, S., deFays, K., Lambert, C., Nakai, K., Brinkman, F.S.L., 2003. PSORT-B: Improving protein subcellular localization prediction for Gram-negative bacteria. Nucleic Acids Res. 31, 3613–3617.

Guo, Z., Thangavel, S., Wang, L., He, Z., Cai, W., Wang, A., Liu, W., 2017. Efficient methane production from beer wastewater in a membraneless microbial electrolysis cell with a stacked cathode: The effect of the cathode/anode ratio on bioenergy recovery. Energy and Fuels 31, 615–620.

He, G., Gu, Y., He, S., Schröder, U., Chen, S., Hou, H., 2011. Effect of fiber diameter on the behavior of biofilm and anodic performance of fiber electrodes in microbial fuel cells. Bioresour. Technol. 102, 10763–10766.

Hernández-Eligio, A., Pat-Espadas, A.M., Vega-Alvarado, L., Huerta-Amparán, M., Cervantes, F.J., Juárez, K., 2020. Global transcriptional analysis of Geobacter sulfurreducens under palladium reducing conditions reveals new key cytochromes involved. Appl. Microbiol. Biotechnol. 104, 4059–4069.

Huang, Q., Liu, Y., Dhar, B.R., 2020. A critical review of microbial electrolysis cells coupled with anaerobic digester for enhanced biomethane recovery from high-strength feedstocks. Crit. Rev. Environ. Sci. Technol.

Kim, K.R., Kang, J., Chae, K.J., 2017. Improvement in methanogenesis by incorporating transition metal nanoparticles and granular activated carbon composites in microbial electrolysis cells. Int. J. Hydrogen Energy 42, 27623–27629.

Klindworth, A., Pruesse, E., Schweer, T., Peplies, J., Quast, C., Horn, M., Glöckner, F.O., 2013. Evaluation of general 16S ribosomal RNA gene PCR primers for classical and next-generation sequencing-based diversity studies. Nucleic Acids Res. 41, e1.

Krylova, N.I., Conrad, R., 1998. Thermodynamics of propionate degradation in methanogenic paddy soil. FEMS Microbiol. Ecol. 26, 281–288.

Li, S., Cheng, C., Thomas, A., 2017. Carbon-Based Microbial-Fuel-Cell Electrodes: From Conductive Supports to Active Catalysts. Adv. Mater. 29, 1602547.

Liu, D., Zheng, T., Buisman, C., Ter Heijne, A., 2017. Heat-Treated Stainless Steel Felt as a New Cathode Material in a Methane-Producing Bioelectrochemical System. ACS Sustain. Chem. Eng. 5, 11346–11353.

Liu, W., Cai, W., Guo, Z., Wang, L., Yang, C., Varrone, C., Wang, A., 2016. Microbial electrolysis contribution to anaerobic digestion of waste activated sludge, leading to accelerated methane production. Renew. Energy 91, 334–339.

Logares, R., Lindström, E.S., Langenheder, S., Logue, J.B., Paterson, H., Laybourn-Parry, J., Rengefors, K., Tranvik, L., Bertilsson, S., 2013. Biogeography of bacterial communities exposed to progressive long-term environmental change. ISME J. 7, 937–948.

Ma, X., Li, Z., Zhou, A., Yue, X., 2017. Energy recovery from tubular microbial electrolysis cell with stainless steel mesh as cathode. R. Soc. Open Sci. 4, 170967.

Morris, R., Schauer-Gimenez, A., Bhattad, U., Kearney, C., Struble, C.A., Zitomer, D., Maki, J.S., 2014. Methyl coenzyme M reductase (mcrA) gene abundance correlates with activity measurements of methanogenic H2/CO2-enriched anaerobic biomass. Microb. Biotechnol. 7, 77.

Noori, M.T., Vu, M.T., Ali, R.B., Min, B., 2020. Recent advances in cathode materials and configurations for upgrading methane in bioelectrochemical systems integrated with anaerobic digestion. Chem. Eng. J. 329, 123689.

Park, Jeong-Hoon, Kang, H.-J., Park, K.-H., Park, H.-D., 2018a. Direct interspecies electron transfer via conductive materials: A perspective for anaerobic digestion applications. Bioresour. Technol. 254, 300–311.

Park, Jeong-Hoon, Park, J.H., Je Seong, H., Sul, W.J., Jin, K.H., Park, H.D., 2018b. Metagenomic insight into methanogenic reactors promoting direct interspecies electron transfer via granular activated carbon. Bioresour. Technol. 259, 414–422.

Park, Jungyu, Lee, B., Shin, W., Jo, S., Jun, H., 2018a. Application of a rotating impeller anode in a bioelectrochemical anaerobic digestion reactor for methane production from high-strength food waste. Bioresour. Technol. 259, 423–432.

Park, Jungyu, Lee, B., Tian, D., Jun, H., 2018b. Bioelectrochemical enhancement of methane production from highly concentrated food waste in a combined anaerobic digester and microbial electrolysis cell. Bioresour. Technol. 247, 226–233.

Rollefson, J.B., Stephen, C.S., Tien, M., Bond, D.R., 2011. Identification of an extracellular

polysaccharide network essential for cytochrome anchoring and biofilm formation in Geobacter sulfurreducens. J. Bacteriol. 193, 1023–1033.

Rotaru, A.-E., Shrestha, P.M., Liu, F., Shrestha, M., Shrestha, D., Embree, M., Zengler, K., Wardman, C., Nevin, K.P., Lovley, D.R., 2014. A new model for electron flow during anaerobic digestion: direct interspecies electron transfer to Methanosaeta for the reduction of carbon dioxide to methane. Energy Environ. Sci. 7, 408–415.

Siegert, M., Li, X.-F., Yates, M.D., Logan, B.E., 2014. The presence of hydrogenotrophic methanogens in the inoculum improves methane gas production in microbial electrolysis cells. Front. Microbiol. 5, 778.

Siegert, M., Yates, M.D., Spormann, A.M., Logan, B.E., 2015. Methanobacterium Dominates Biocathodic Archaeal Communities in Methanogenic Microbial Electrolysis Cells. ACS Sustain. Chem. Eng. 3, 1668–1676.

Stöckl, M., Teubner, N.C., Holtmann, D., Mangold, K.M., Sand, W., 2019. Extracellular Polymeric Substances from Geobacter sulfurreducens Biofilms in Microbial Fuel Cells. ACS Appl. Mater. Interfaces 11, 8961–8968.

Tan, B., Zhou, S.F., Wang, Y., Zhang, B.P., Zhou, L.H., Yuan, Y., 2019. Molecular insight into electron transfer properties of extracellular polymeric substances of electroactive bacteria by surface-enhanced Raman spectroscopy. Sci. China Technol. Sci. 62, 1679–1687.

Tian, T., Qiao, S., Yu, C., Zhou, J., 2019. Effects of nano-sized MnO2 on methanogenic propionate and butyrate degradation in anaerobic digestion. J. Hazard. Mater. 364, 11–18.

Villano, M., Aulenta, F., Ciucci, C., Ferri, T., Giuliano, A., Majone, M., 2010. Bioelectrochemical reduction of CO2 to CH4 via direct and indirect extracellular electron

transfer by a hydrogenophilic methanogenic culture. Bioresour. Technol. 101, 3085–3090.

Villano, M., Ralo, C., Zeppilli, M., Aulenta, F., Majone, M., 2016. Influence of the set anode potential on the performance and internal energy losses of a methane-producing microbial electrolysis cell. Bioelectrochemistry 107, 1–6.

Wang, J., Li, M., Liu, F., Chen, S., 2016. Stainless Steel Mesh Supported Carbon Nanofibers for Electrode in Bioelectrochemical System. J. Nanomater. 2016.

Wilkins, D., Lu, X.Y., Shen, Z., Chen, J., Lee, P.K.H., 2015. Pyrosequencing of mcrA and archaeal 16s rRNA genes reveals diversity and substrate preferences of methanogen communities in anaerobic digesters. Appl. Environ. Microbiol. 81, 604–613.

Wormald, R., Humphreys, P., 2019. Hydrogenotrophic methanogenesis dominates at high pH. Access Microbiol. 1, 169.

Xiao, Y., Zhang, E., Zhang, J., Dai, Y., Yang, Z., Christensen, H.E.M., Ulstrup, J., Zhao, F., 2017. Extracellular polymeric substances are transient media for microbial extracellular electron transfer. Sci. Adv. 3, e1700623.

Xu, H., Wang, K., Holmes, D.E., 2014. Bioelectrochemical removal of carbon dioxide (CO2): An innovative method for biogas upgrading. Bioresour. Technol. 173, 392–398.

Yang, G., Huang, L., Yu, Z., Liu, X., Chen, S., Zeng, J., Zhou, S., Zhuang, L., 2019. Anode potentials regulate Geobacter biofilms: New insights from the composition and spatial structure of extracellular polymeric substances. Water Res. 159, 294–301.

Ye, J., Hu, A., Ren, G., Chen, M., Tang, J., Zhang, P., Zhou, S., He, Z., 2018. Enhancing sludge methanogenesis with improved redox activity of extracellular polymeric substances by hematite in red mud. Water Res. 134, 54–62.

Yu, H.Q., 2020. Molecular Insights into Extracellular Polymeric Substances in Activated Sludge. Environ. Sci. Technol. 54, 7742–7750.

Zakaria, B.S., Dhar, B.R., 2021. An intermittent power supply scheme to minimize electrical energy input in a microbial electrolysis cell assisted anaerobic digester. Bioresour. Technol. 319, 124109.

Zakaria, B.S., Dhar, B.R., 2020. Changes in syntrophic microbial communities, EPS matrix, and gene-expression patterns in biofilm anode in response to silver nanoparticles exposure. Sci. Total Environ. 734, 139395.

Zakaria, B.S., Dhar, B.R., 2019. Progress towards catalyzing electro-methanogenesis in anaerobic digestion process: Fundamentals, process optimization, design and scale-up considerations. Bioresour. Technol. 289, 121738.

Zakaria, B.S., Lin, L., Chung, T., Dhar, B.R., 2020. An overview of complementary microbial electrochemical technologies for advancing anaerobic digestion. Elsevier, pp. 129–167.

Zakaria, B.S., Lin, L., Dhar, B.R., 2019. Shift of biofilm and suspended bacterial communities with changes in anode potential in a microbial electrolysis cell treating primary sludge. Sci. Total Environ. 689, 691–699.

Zhang, L., Zhu, X., Li, J., Liao, Q., Ye, D., 2011. Biofilm formation and electricity generation of a microbial fuel cell started up under different external resistances. J. Power Sources 196, 6029–6035.

Zheng, L., Zhang, Z., Tian, L., Zhang, L., Cheng, S., Li, Z., Cang, D., 2019. Mechanistic investigation of toxicological change in ZnO and TiO2 multi-nanomaterial systems during anaerobic digestion and the microorganism response. Biochem. Eng. J. 147, 62–71.

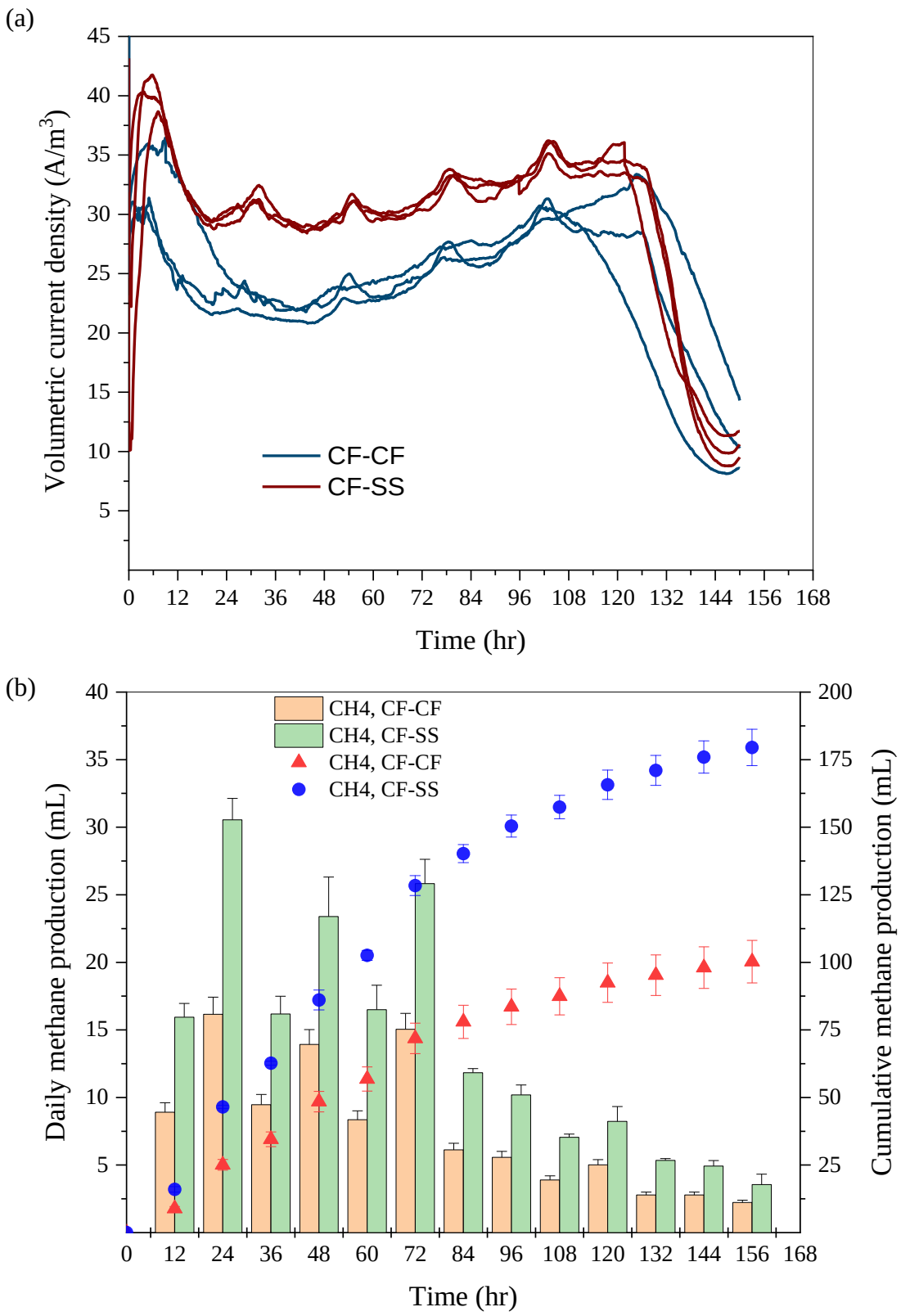

Fig. 1. Volumetric current density (a), and methane production (b) from CF-CF and CF-SS reactors.

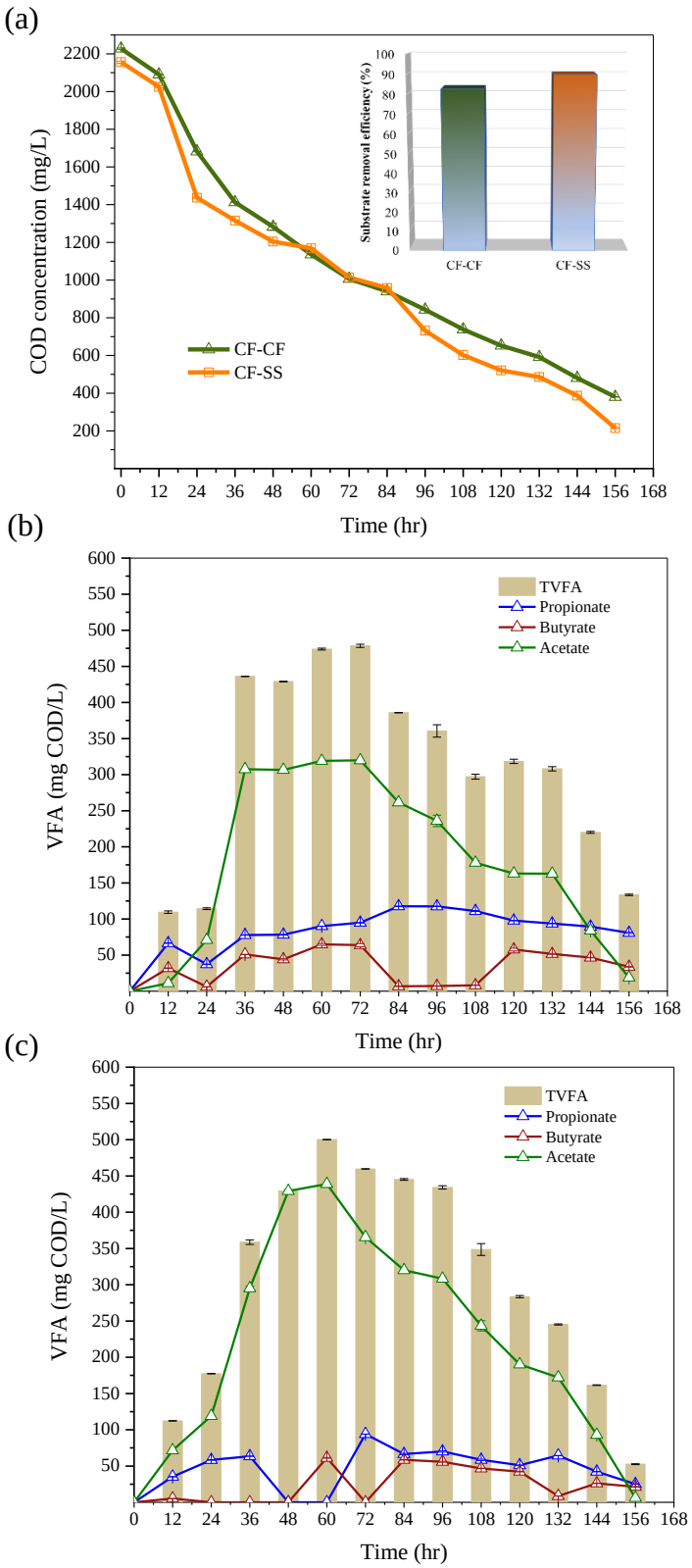

Fig. 2. COD concentration (a), and VFA profiles (b, c) in CF-CF and CF-SS reactors.

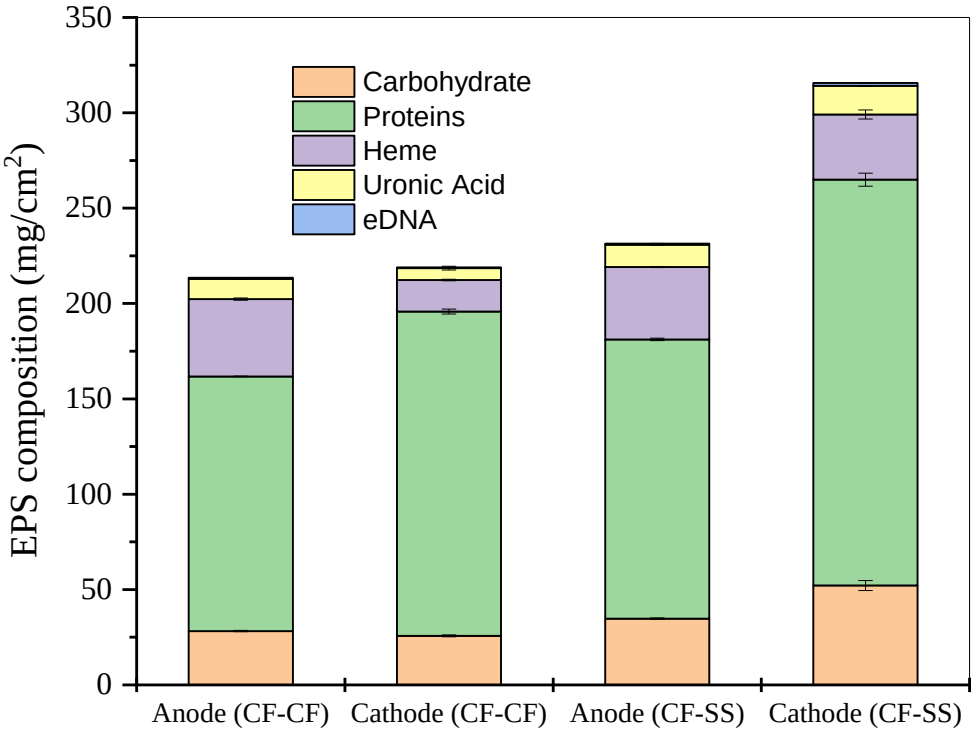

Fig. 3. EPS composition of CF-CF and CF-SS reactors.

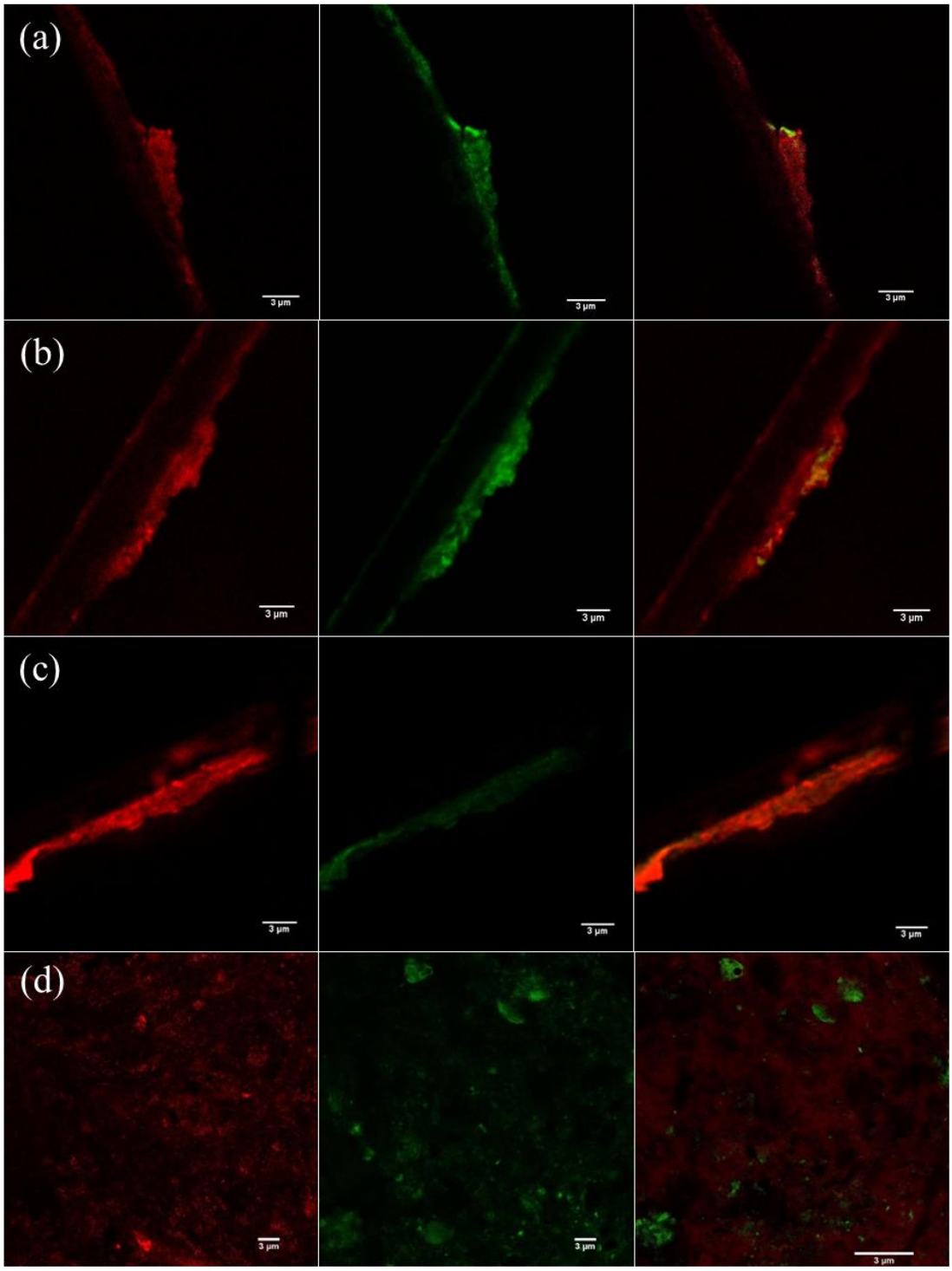

Fig. 4. Confocal microscopic images of EPS with 3 µm scale; Anode (CF-CF) (a), cathode (CF-CF) (b), Anode (CF-SS) (c), and cathode (CF-SS) (d).

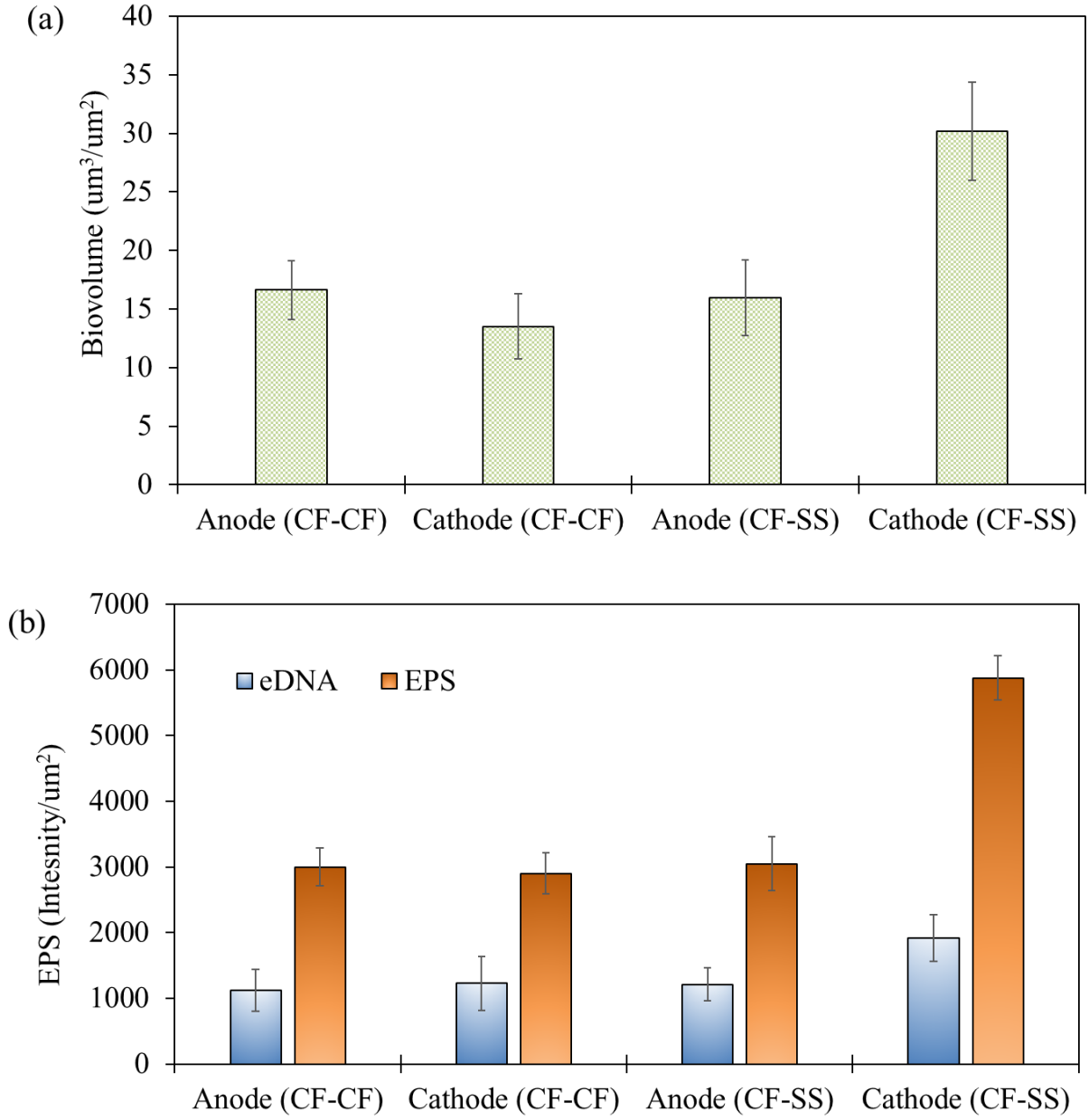

Fig. 5. EPS quantitative analysis using CLSM; biovolume (a), and fluorescence intensity (b).

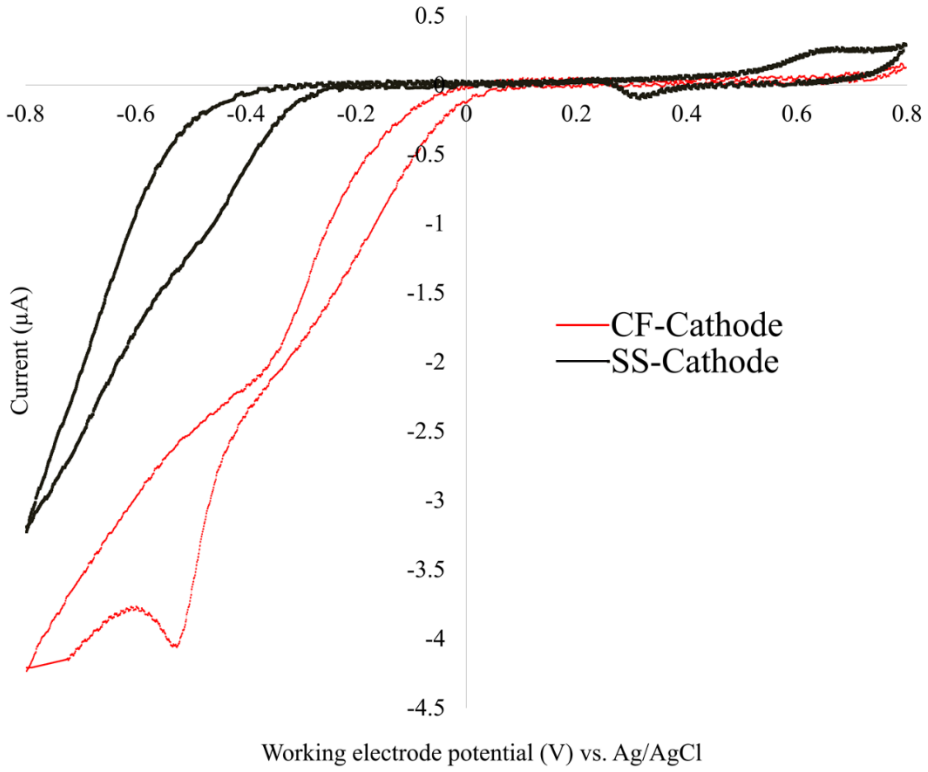

Fig. 6. Cyclic voltammetry of EPS extracted from biocathode in CF-CF and CF-SS reactors.

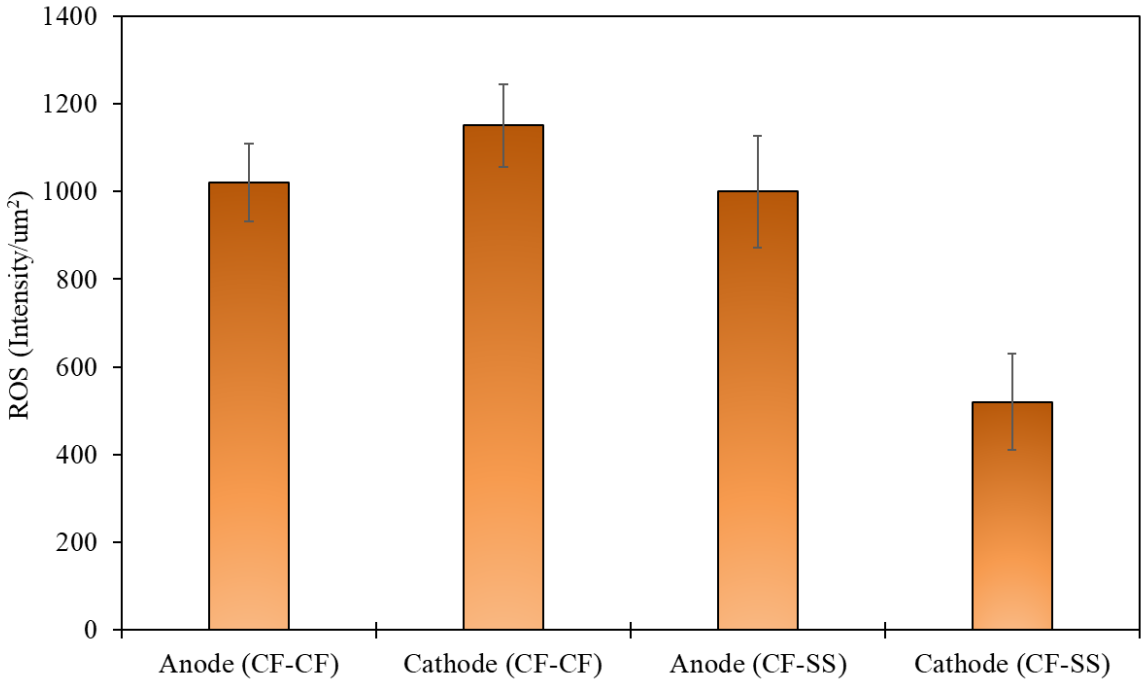

Fig. 7. Reactive oxygen species (ROS) intensities in CF-CF and CF-SS biofilms.

(a)

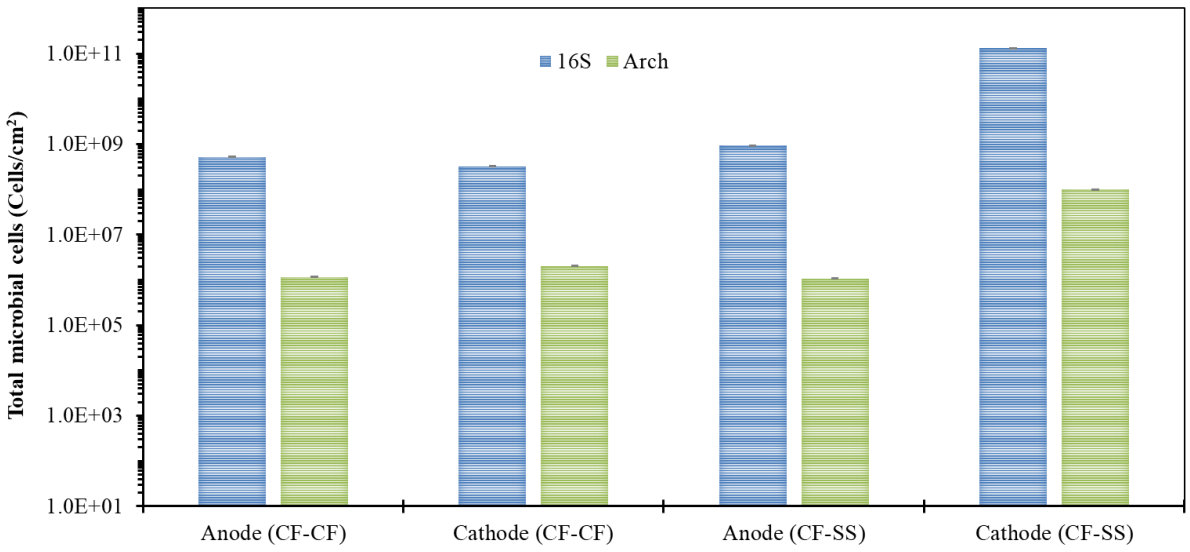

(b)

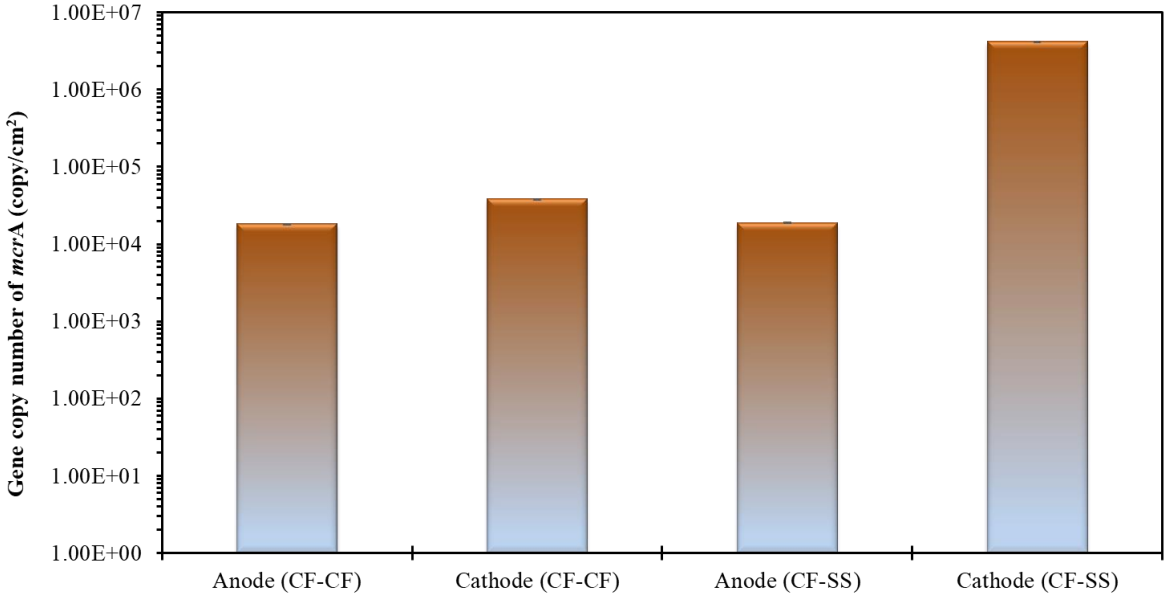

Fig. 8. Total cell number using 16s and archaeal primers (a), and *mcr*A gene copies (b).

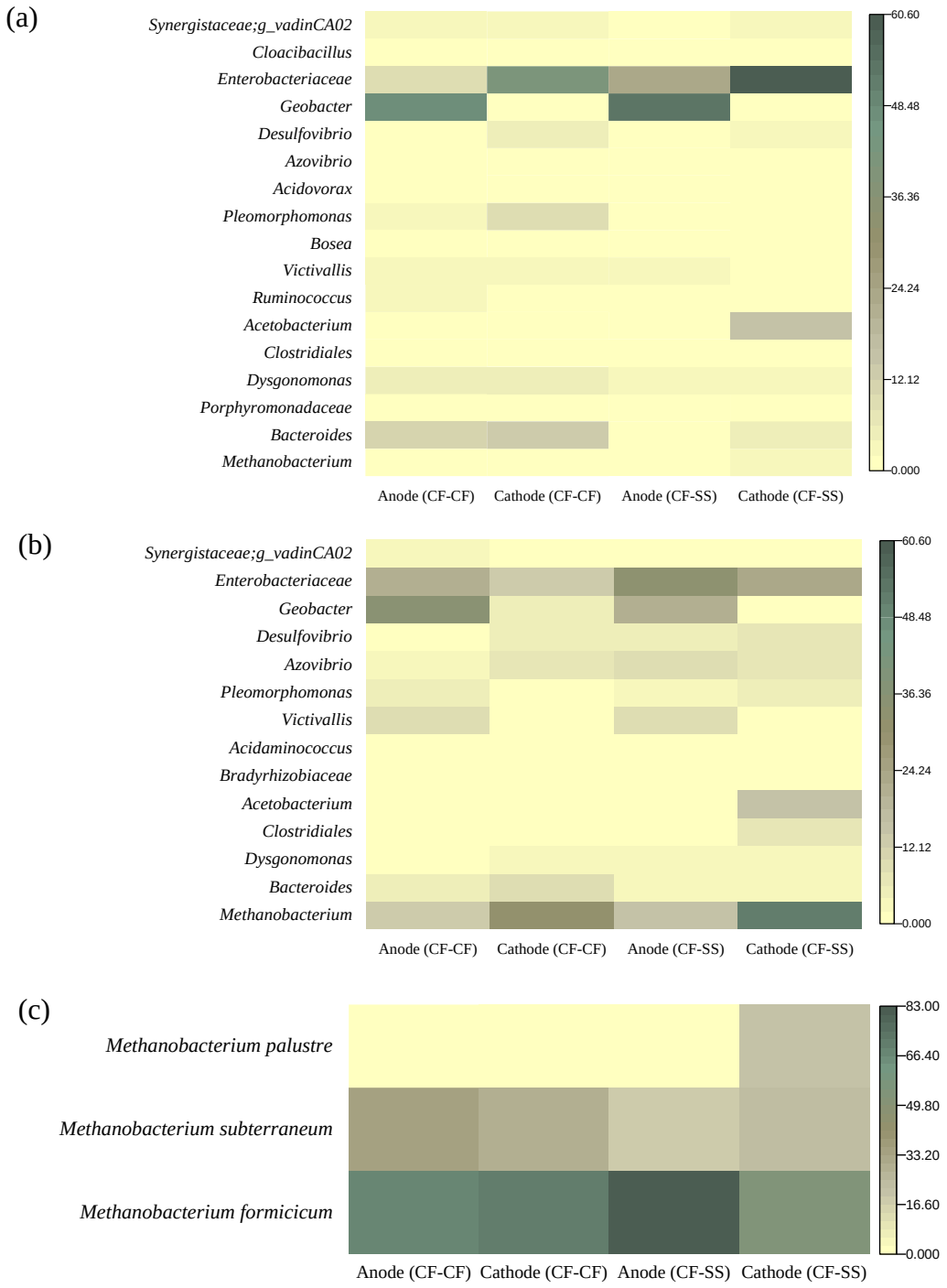

Fig. 9. Relative abundance of microbial communities analyzed with bacterial primer (a), archaeal primer (b), and *mcr*A primer (c) at the genus level.

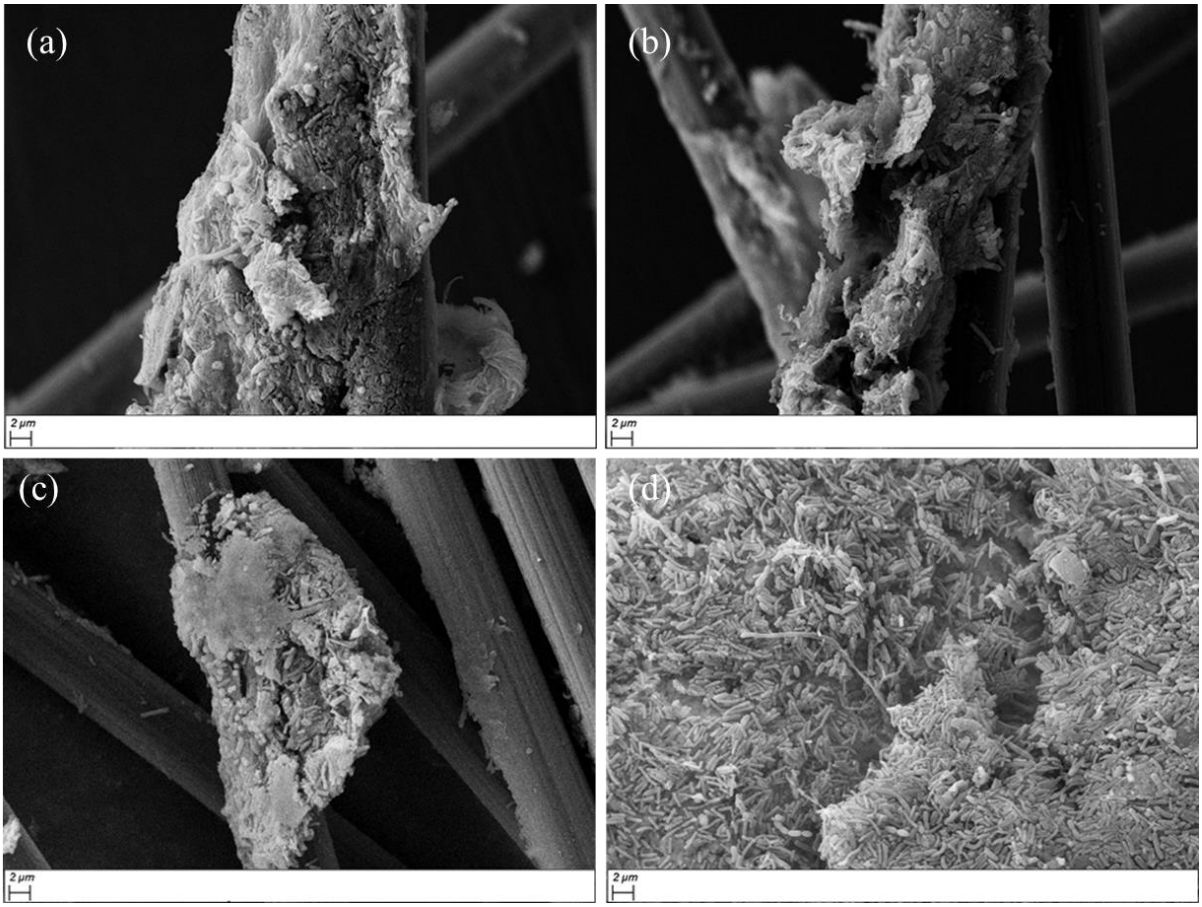

Fig. 10. SEM images of biofilms developed on anode (CF-CF) (a), cathode (CF-CF) (b), anode (CF-SS) (c), and cathode (CF-SS) (d).

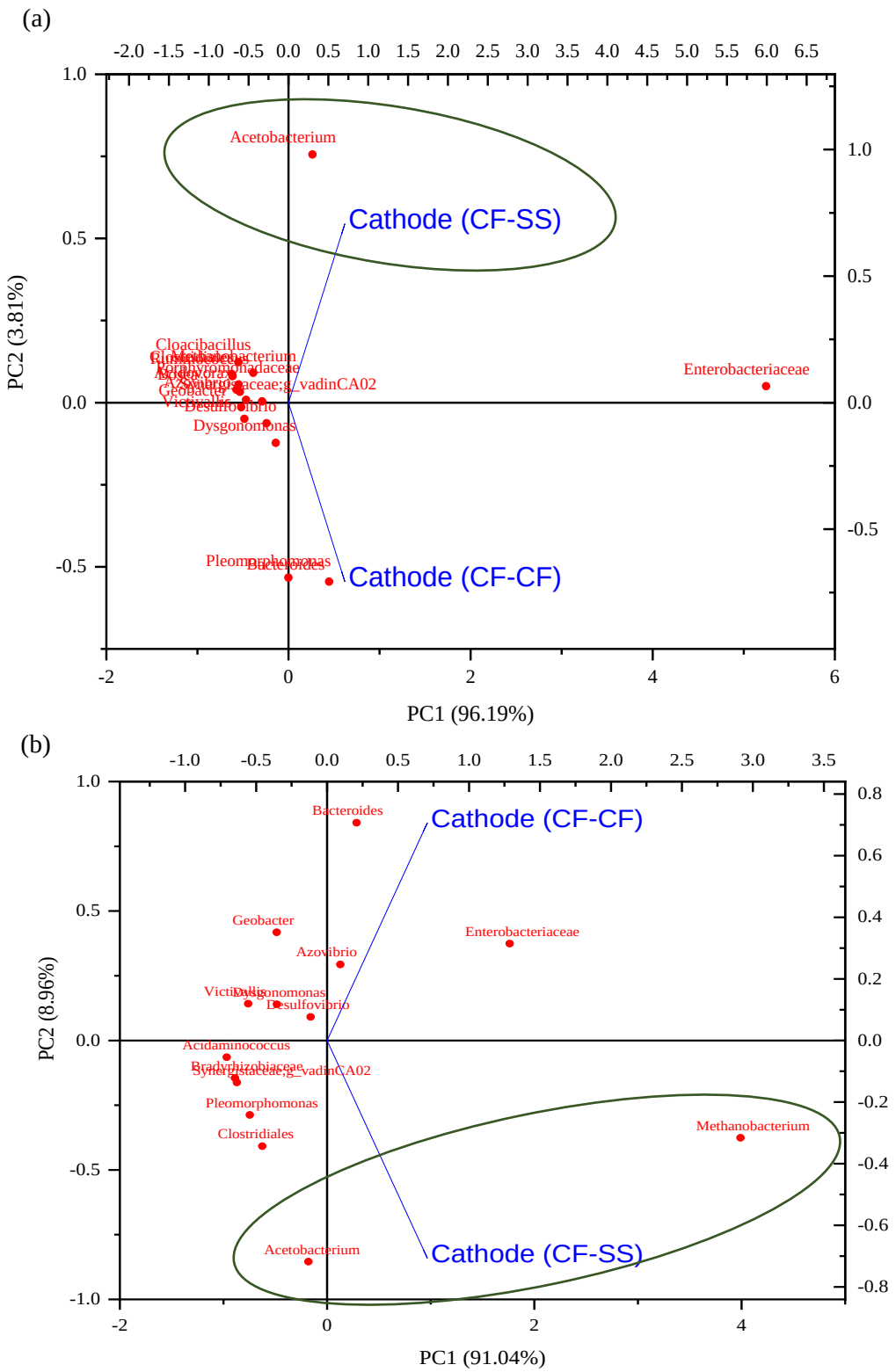

Fig. 11. Principal Component Analysis of the bacterial (a) and archaeal (b) communities in biocathode of CF-CF and CF-SS reactors.

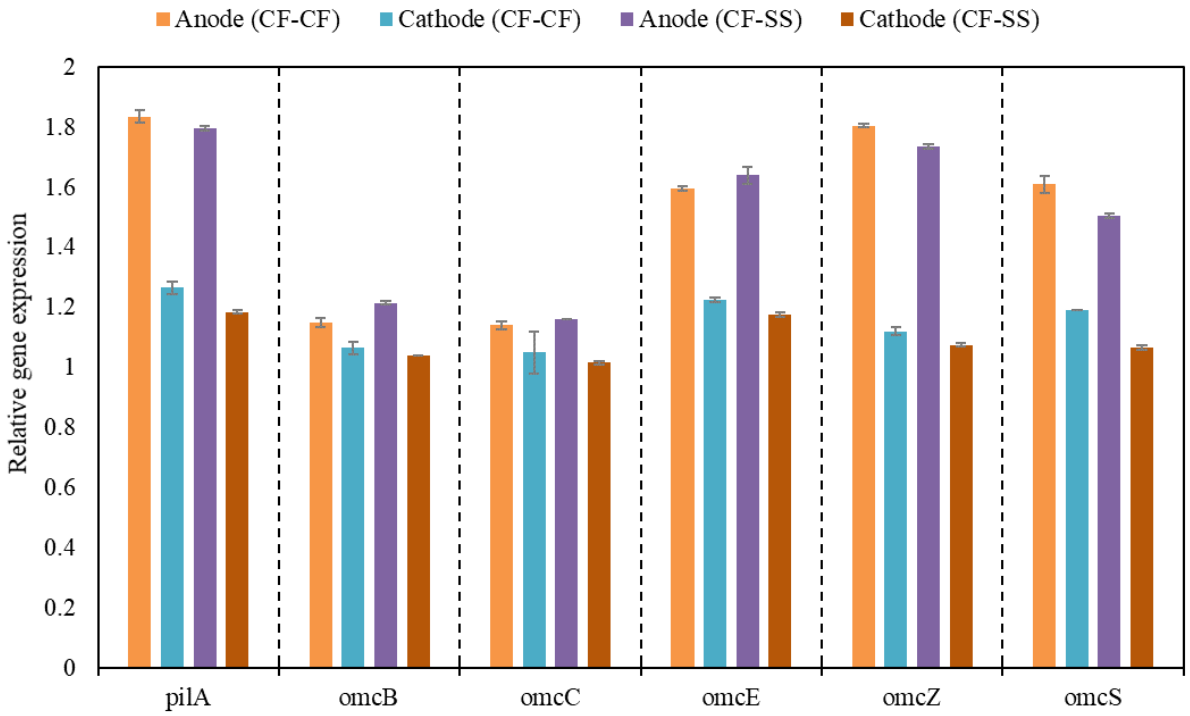

Fig. 12. Expression of genes known to regulate extracellular electron transfer in biofilms.